



Controllability of pore size on macroporous sol-gel silica films embedding rhodamine 6G

J. Castañeda-Contreras^{a*} • H. Pérez Ladrón de Guevara^a • M. A. Meneses-Nava^b
V. F. Marañón-Ruiz^a • R. Chiu-Zarate^a • R. Rodríguez-Rojas^a • R. J. Patakfalvi^a

^aUniversidad de Guadalajara, C.U. de los Lagos. Lagos de Moreno, Jalisco. México

^bCentro de Investigaciones en Óptica, A.C. León Guanajuato, México.

Received 06 11 2019; accepted 01 21 2021

Available 04 30 2021

Abstract: A facile method is reported to synthesize macroporous silica films embedding rhodamine 6G. The films were obtained by sol-gel and spin-coating processes. Results pointed out a dependence of pore formation on the addition of rhodamine 6G in the film composition. The probable formation process of the pores was attributed to the aggregation of charged species from rhodamine 6G. Although the pores were randomly distributed on the film surface, the pore size was tuned at certain extent by controlling the evaporation and condensation rates at early stages of spin coating. Results indicated that the evaporation rate determined the pore size distribution of the films.

Keywords: Silica, sol-gel, spin coating, macro pores

*Corresponding author.

E-mail address: jcc050769@yahoo.com.mx (J. Castañeda-Contreras).

Peer Review under the responsibility of Universidad Nacional Autónoma de México.

1. Introduction

Currently, there is an increasing interest on developing porous solids because of their ability to interact with atoms, ions and molecules in applications that involve ion exchange, filters, photo catalysts, environmental applications, solar fuels, adsorption of organic molecules such as DNA, etc.

(Ashrafi-Shahri, Ravari & Seifzadeh, 2019; Bhar et al., 2020; Herzog et al., 2020; Phan et al., 2019; Roushani & Ghanbari, 2019; Wu et al., 2019; Yamashita et al., 2018; Yang et al., 2019). The distribution of sizes and shapes of the pores directly relates to their ability to perform the desired function in a particular application. The synthesis procedures for porous materials are broadly focused on lithographic techniques (Zhang et al., 2017) and self-assembly (Li et al., 2020). For the latter, building blocks acting as templates that organize themselves into functional structures depending if the species are charged or not (Bao et al., 2017). On the other hand, porous materials are often synthesized as thin films. The sol-gel route is a major technique used to prepare these films. This technique generally involves wet chemical coatings of sol-gel solutions on a substrate by dip, spray or spin coating (Gaspera & Martucci, 2015). The influence of evaporation rate of solvents is an additional key parameter that might determine the final structure (Gibaud et al., 2003). The incorporation of fluorescent dyes such as rhodamine 6G (Rh6G) to sol-gel silica materials are of great interest because of their photoluminescence applications (Leonenko et al., 2015). However, in this work we report the addition of Rh6G to promote the pore formation. The aggregation processes of organic dyes determine their optical properties; these are well characterized so far (Malfatti et al., 2008). In this work, we proposed a facile method to obtain porous films by the addition of Rh6G at early stages of sol-gel process. During the synthesis, the Rh6G formed H-dimers and monomeric species. These aggregates acted as structure-directing agents in our films. Once the samples were obtained, the Rh6G is easily photo-bleached by irradiation with visible light, obtaining a transparent film. Despite the complexity of the related mechanisms, we present a first insight of the role of the evaporation rate on the pore formation. To the best of our knowledge, there are not reports related to control the pore size by the solvent evaporation rate on sol-gel silica films, furthermore, most works in the literature utilize surfactants and other species as templates to promote the pore formation.

2. Materials and methods

All chemicals were purchased from Sigma-Aldrich Inc., and utilized as received without further purification. Sol-gel silica films were synthesized with tetra-ethoxysilane (TEOS) as SiO₂ precursor. TEOS was first dissolved in ethanol (EtOH) under

vigorous magnetic stirring. After an hour, an alcoholic solution of rhodamine 6G (Rh6G) and a solution of hydrochloric acid in distilled water were added to hydrolyze the precursor. The corresponding molar ratios were: TEOS 1: H₂O 4: HCl 0.05: Rh6G 1×10^{-3} : EtOH x ; where x is related to molar ratios: 2, 4 and 6. The sol was left at room temperature for 24 hours. Microscope slides were utilized as substrates. These were previously cleaned by sonication in an ultrasonic bath, rinsed with distilled water and dried in an oven at 250° C. Subsequently, 60 micro-liters of the sol were deposited on a substrate. It was placed in a spin-coater from Chemat. After the spinning process, the samples were heated at 90° C during 30 minutes on a hot plate to promote film densification. Thickness of the films was measured with a Thin Film Analyzer (Filmetrics F20). The thin film surface morphology was studied with an Atomic Force Microscopy (Nanosurf Easyscan 2), which had a 70 μm head. We utilized a standard silicon tip in AFM measurements, with imaging mode via static force (contact). The tip voltage was set at ±10 V in 5 mV steps. Five measurements were made on each sample at various positions. The error in the measurements due to XY-linearity of AFM was < 1.2 %. The absorption spectra of the Rh6G doped silica films were recorded with a spectrometer QE65000 and a deuterium-halogen lamp from Ocean Optics.

3. Results and discussion

3.1. Macro pores formation on a sol-gel silica thin film with Rh6G

We fabricated two silica films: one of them had Rh6G and the other was synthesized without this dye. The EtOH molar ratios were fixed at 4 for both samples. The spin-coating speed was set at 1200 rpm for 30 s. The measured thickness of the films was averaged at ~190 nm. Figure 1(a) shows macro pores on the film with Rh6G, and Figure 1(b) shows the absence of pores on the film surface without Rh6G. Therefore, the dye addition in our silica films was responsible for the pore formation.

The size distribution of the macro pores was taken by measuring the Feret's diameter from the corresponding AFM images. The size distribution of the pore is shown in Figure 2, where the peak of the size distribution was located at 860 nm

3.2. Macro pores on sol-gel silica thin film doped with Rh6G at different spin-coating speed

The overlap on deposition and drying stages of the spin-coating process establishes a competition between evaporation (which compacts a sol-gel film), and condensation reactions (which solidifies the film). Thus, film porosity has a strong dependence on the relative rates of condensation and evaporation. In order to study the effect of

solvent evaporation, two thin films with Rh6G were deposited at different speeds: 900 rpm and 1800 rpm. The ETOH molar ratio of the sol was fixed at 4. As expected, the film thickness decreased for higher rpm, thus at 900 rpm the measured thickness was ~ 221 nm; whereas at 1800 rpm the corresponding thickness was averaged at ~ 128 nm, respectively. Figure 3 shows AFM micrographs of the films deposited at (a) 900 rpm and (b) 1800 rpm, where is clear that the pore diameter is larger for the former. The corresponding size distribution of the pores is shown in Figure. 4 (a) at 900 rpm, the peak of the size distribution was 1495 nm, and (b) at 1800 rpm, the peak shifted to 610 nm.

The difference on the pore diameter is attributed to a slower evaporation ratio of the sample at lower rotation speed, compared to the rapid drying of the film deposited at higher rpm. Therefore, the solvent evaporation rate at 900 rpm allowed the formation of wider macro structures. In the other hand, the film at 1800 rpm is expected to be solidified at early stages of the spin-coating process, because the higher solvent evaporation rate at increased speeds. Thus, at 1800 rpm the pores shown a reduced diameter in comparison to these at 900 rpm, as shown in Figure. 4. This behavior is similar to the reported by Pan and Lee (2005), where authors control the pore morphology by varying spin coating speed.

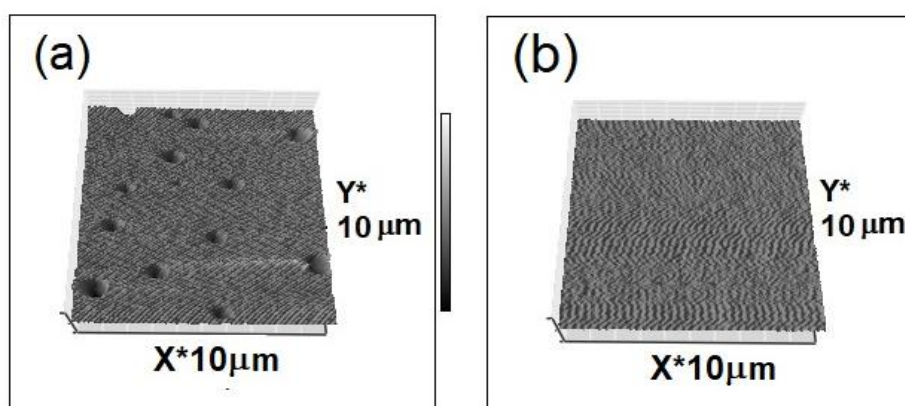


Figure 1. AFM micrographs from sol-gel silica films: (a) With the addition of Rh6G during the synthesis and (b) pure silica film without Rh6G.

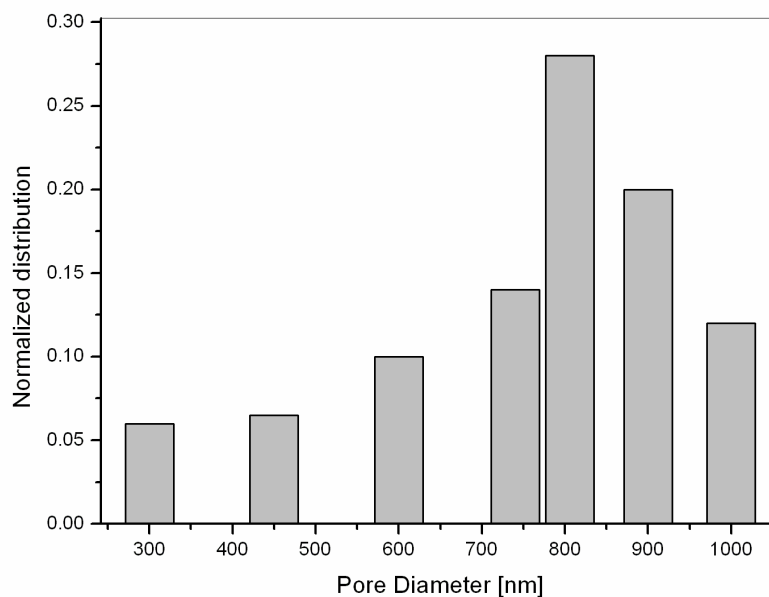


Figure 2. Size distribution of pore diameters of sol-gel silica film with ETOH molar ratio of 4.

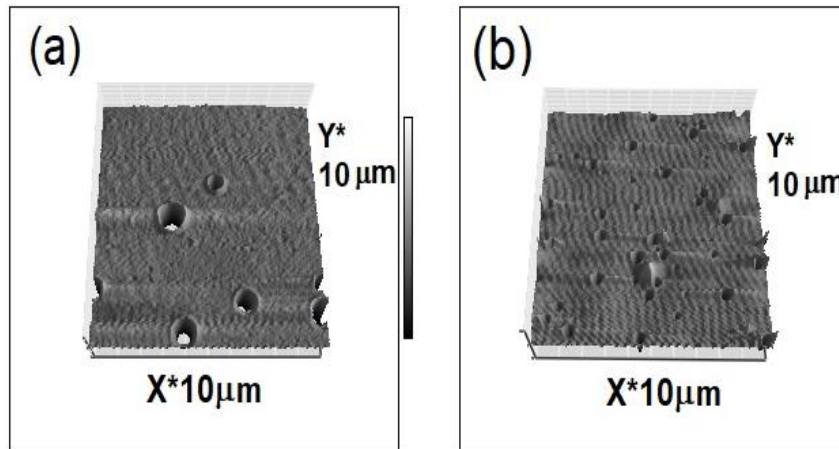


Figure 3. AFM micrographs of the surface morphology of silica thin films synthesized at different spin-coating speed: (a) 900 rpm, and (b) 1800 rpm.

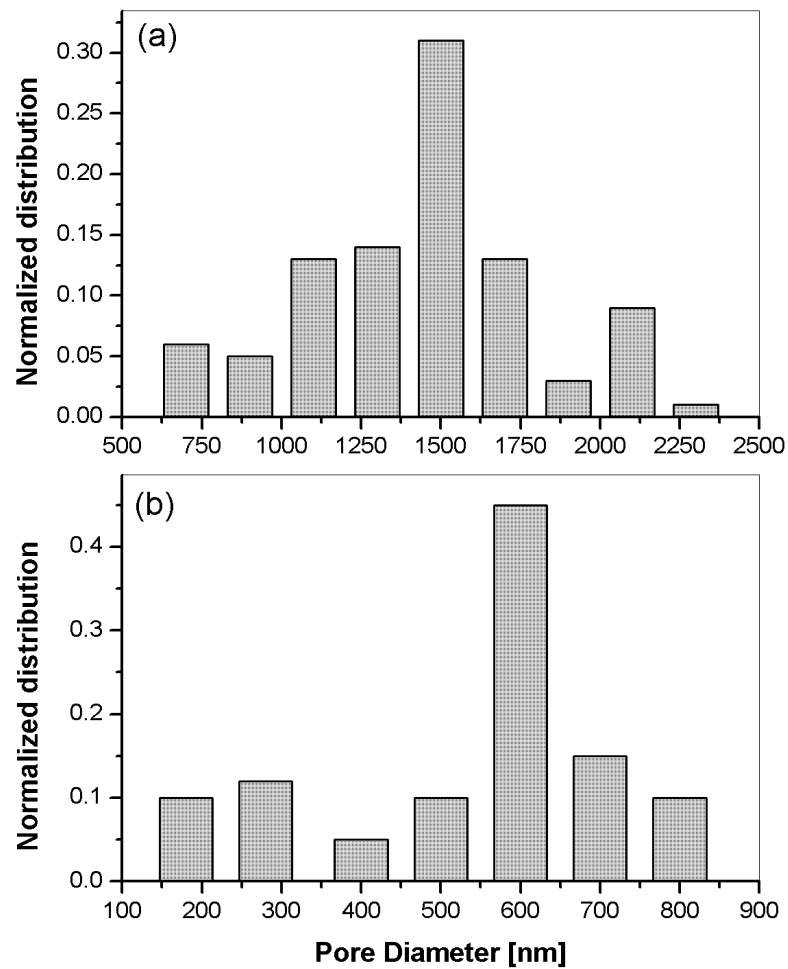


Figure 4. Size distribution of pore diameters on sol-gel silica films with Rh6G synthesized at different spin-coating speeds: (a) 900 rpm, and (b) 1800 rpm. The ETOH molar ratio was fixed at 4.

3.3. Rh6G-doped silica films at different ETOH molar ratio

During sol-gel process, the hydrolysis of the precursor is favored when ETOH is added to prevent phase separation of immiscible H₂O with the silica precursor and to control the concentration of H₂O and silicate that influence the gelation kinetics. With the aim to study the role of ETOH content in the pore size, we fabricated two sets of silica films at different ETOH content: a set with an ETOH molar ratio fixed at 6 (ETOH: 6); and other at ETOH molar ratio of 2 (ETOH: 2). The films from ETOH: 6 were obtained at zero rpm, 900 rpm and 1800 rpm. The different rpm was intended to test the effect of ETOH evaporation on pore size. The AFM images from this set are shown in Figure 5. The film at zero rpm (Figure 5a), was obtained as described on section 3.1. It was denoted as a thick film because its thickness was averaged at ~23 μm. This film, although with several fractures on its surface, exhibited the largest pores. Some of them had a diameter up to 17.4 μm. On the other hand, the films obtained at 900 rpm and 1800 rpm (figures 5b and 5c) had smaller pore sizes, and had averaged thicknesses of ~103 nm and ~98 nm, respectively.

Figure 6 shows pore size distribution plots from the aforementioned set. The peak size distribution for the zero rpm film was 2580 nm, as depicted on graph 6(a). At 900 rpm,

the peak was 1697 nm, whereas at 1800 rpm, the peak shifted to 898 nm, as shown on graphs 6(b) and 6(c), respectively. By comparing the pore size distribution with the measured film thickness, there is an indication that the evaporation rate is the main variable that determines the pore size, similarly to that reported by Gibaud et al. (2003) for surfactant templated silica mesophases.

The set from ETOH: 2 were deposited at 900 rpm and 1800 rpm. We failed to obtain a film at zero rpm; it was completely fractured, probably as a result of the relatively low ETOH content. The film thickness of the film at 900 rpm was averaged at ~220 nm, and the corresponding to 1200 rpm was ~142 nm. The pore size distribution of this set is shown on Figure 7. The graph on 7(a) shows that the peak size for the film deposited at 900 rpm was 580 nm; whereas the film at 1800 rpm had a shifted peak size of 321 nm, as shown on graph 7 (b). By comparing the pore size distribution of the films at different ETOH content, we inferred the increased ETOH content led to a reduction of the viscosity of the solution, leading to larger pore diameters.

Therefore, according to the above results, we proposed that pore size can be tuned at certain extent by controlling the evaporation rate. This was accomplished by varying both the ETOH content and the spin-coating rpm. Those aspects are summarized on Figure 8.

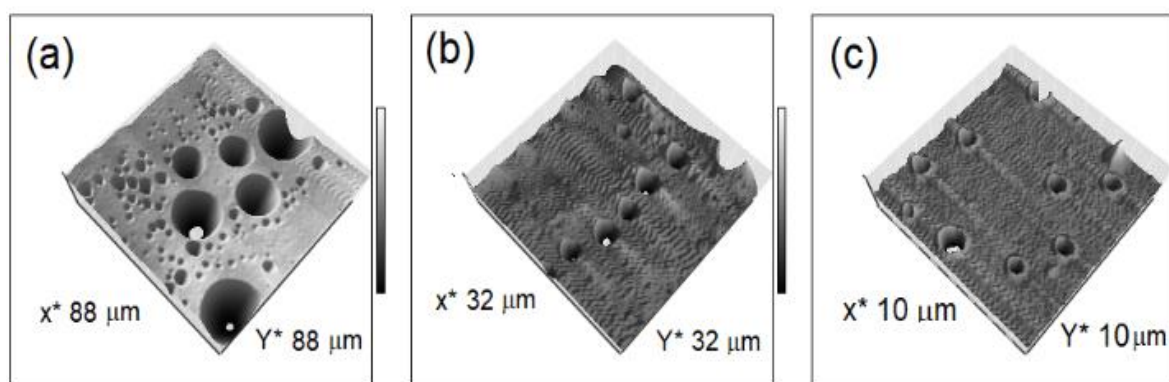


Figure 5. AFM micrographs of the surface morphology of sol-gel silica films synthesized with an ETOH molar ratio of 6. The corresponding spin-coating speeds were (a) zero rpm, (b) 900 rpm, (c) 1800 rpm.

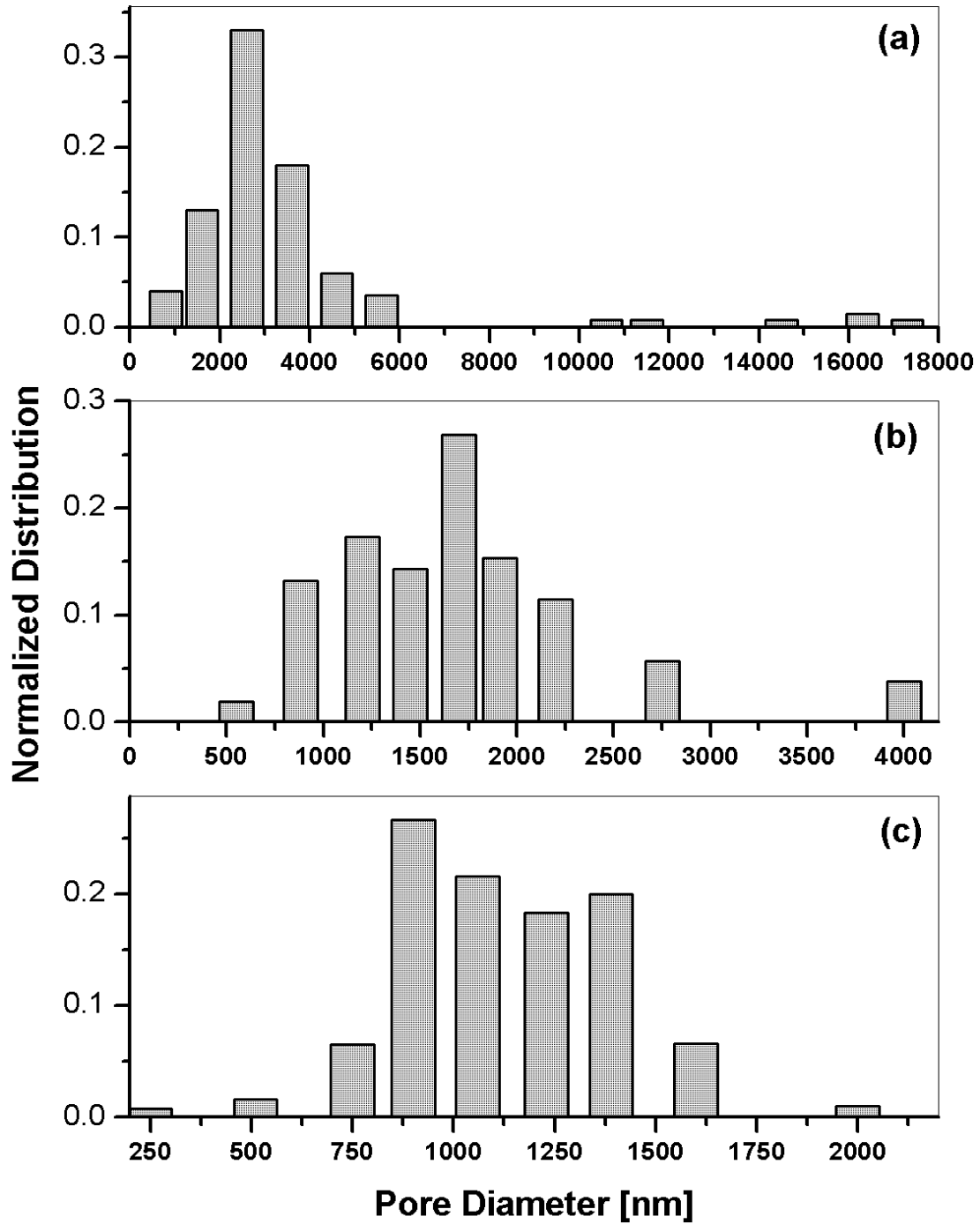


Figure 6. Size distribution of pore diameters on sol-gel silica films synthesized at different spinning speeds: (a) zero rpm, (b) 900 rpm and (c) 1800 rpm.

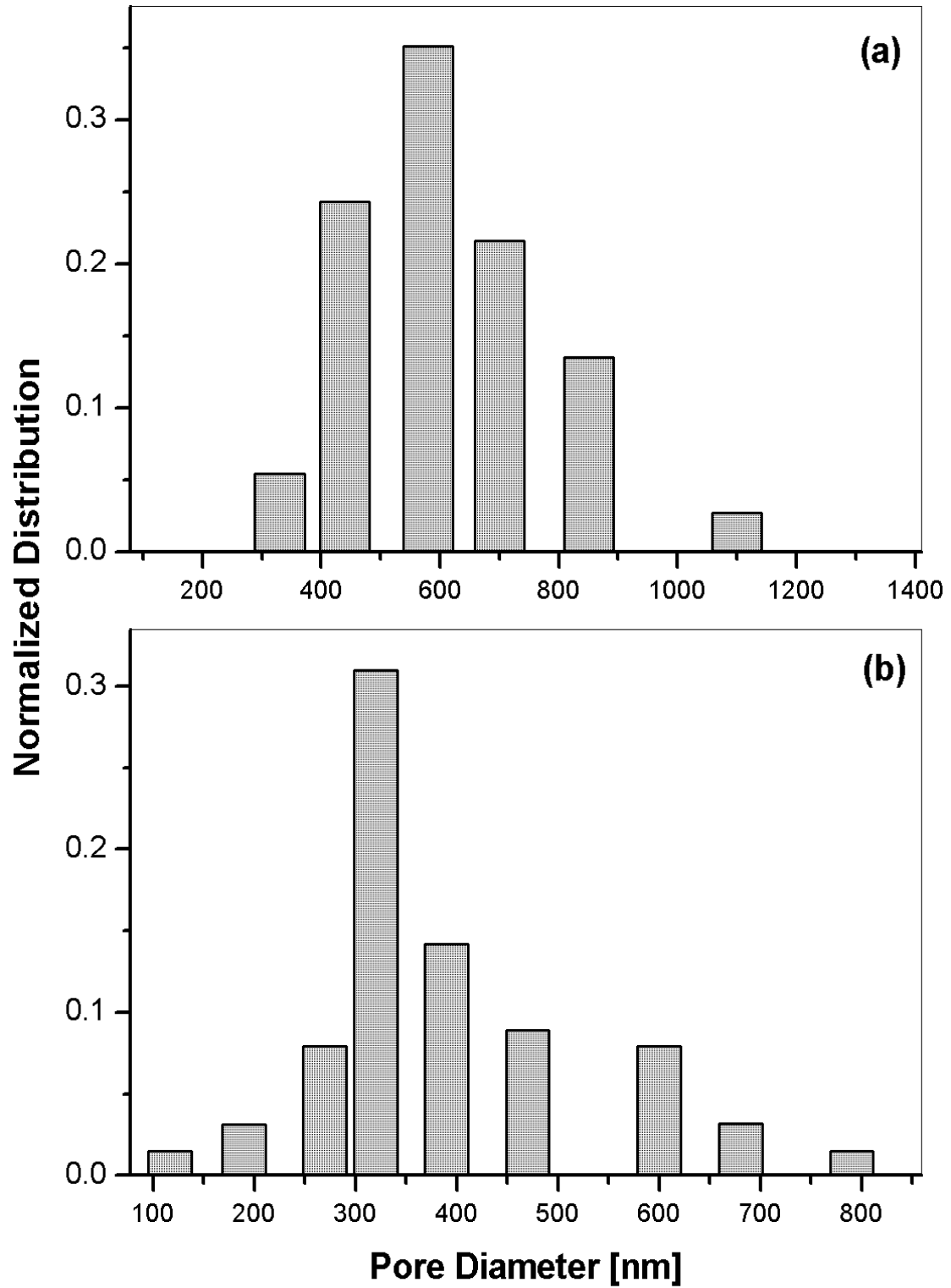


Figure 7. Size distribution of pore diameters on sol-gel silica thin films at different spinning speeds: (a) 900 rpm, (b) 1800 rpm. The ETOH molar ratio on these films was fixed at 2.

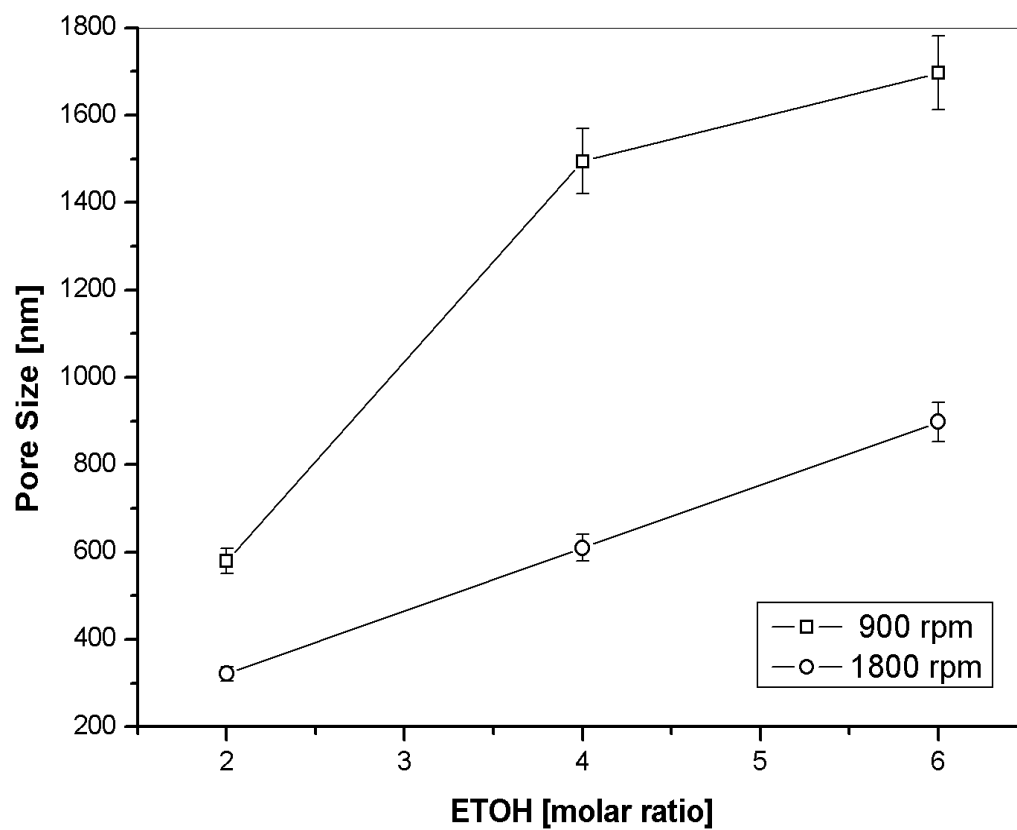


Figure 8. Effect of the spin-coating speed and ETOH content on pore diameters of macroporous sol-gel silica thin films with Rh6G. The depicted pore sizes correspond to the peaks of size distribution.

3.4. Aggregates of Rh6G

The pore sizes described above are away from the size from molecular templates, which are usually in the 2-50 nm range (Corma, 1997). Thus, Rh6G as a template is an unlikely explanation for the pore formation. We suggest that a probable mechanism for pore formation was the aggregation of the dye, where silica species and monomeric Rh6G acted as building blocks. These effects are most pronounced in thin films where, because of evaporation, chromophores tend to self-assemble into higher order structures, as described by Hanczyc et al. (2015). Thus, as reported in the literature so far, we speculate that the addition of a positively charged dye such as Rh6G (Mubarekyan & Santore, 1998) added a certain amount of charge to the sol-gel reaction. This resulted in pore formation, probably by an assembly-type mechanism of the silica species. However, work is in progress to clarify this point.

On the other hand, Nishikiori and Fuji (1997), report that Rhodamine B shows a strong tendency to form dimers inside sol-gel silica films. These dimers, namely H-type or J-type are

identified by an increase of the dye absorption bands located at 500 nm and 590 nm, respectively (Nasr et al., 1997). Similar dimers appeared in Rh6G-doped sol-gel silica films (Narang et al., 1994). Figure 9 shows the absorption spectra of the films at 2, 4 and 6 ETOH content for different spin-coating speeds: (a) 900 rpm and (b) 1800 rpm. These spectra depict a rise of the 500 nm peak for the films at ETOH:6 and ETOH:4 for 1800 RPM; a similar behavior is shown on the spectrum for ETOH:6 in Figure 9(b) for 900 RPM. This absorption band at 500 nm is related to H-type dimer, whereas the peak at 530 nm is assigned to the monomeric form of Rh6G.

These results pointed out that monomeric Rh6G was the preferential aggregate in our samples; whereas H-type dimer has a dependence of solvent content, similarly to the reported by Leonenko et al. (2015) for hybrid mesostructured silica films. This suggests that besides the formation of larger pore diameters, the variables of synthesis such as evaporation rates and higher ETOH content also favored the formation of

H-dimers at certain extent. However, is not conclusive that these aggregates produced larger pores, our experimental results pointed out that the main variable was the evaporation rate. This is shown on [Figure 9\(b\)](#), where the plot of ETOH:6 at 1800 rpm pointed out a higher content of H-dimers when compared to the other films. Nevertheless, the larger pores were recorded on the film of ETOH:6 at 900 rpm, as explained above.

Since most applications for porous films require hosts with neutral optical properties, the Rh6G embedded in our samples must be deactivated. This was accomplished by just irradiating for 12 h the samples with an 80W ordinary fluorescent lamp. It was placed 30 cm above the films. This resulted in the photo bleaching of the dye, leaving the pores intact and suitable to act a mechanical host in applications that require immobilized species in them.

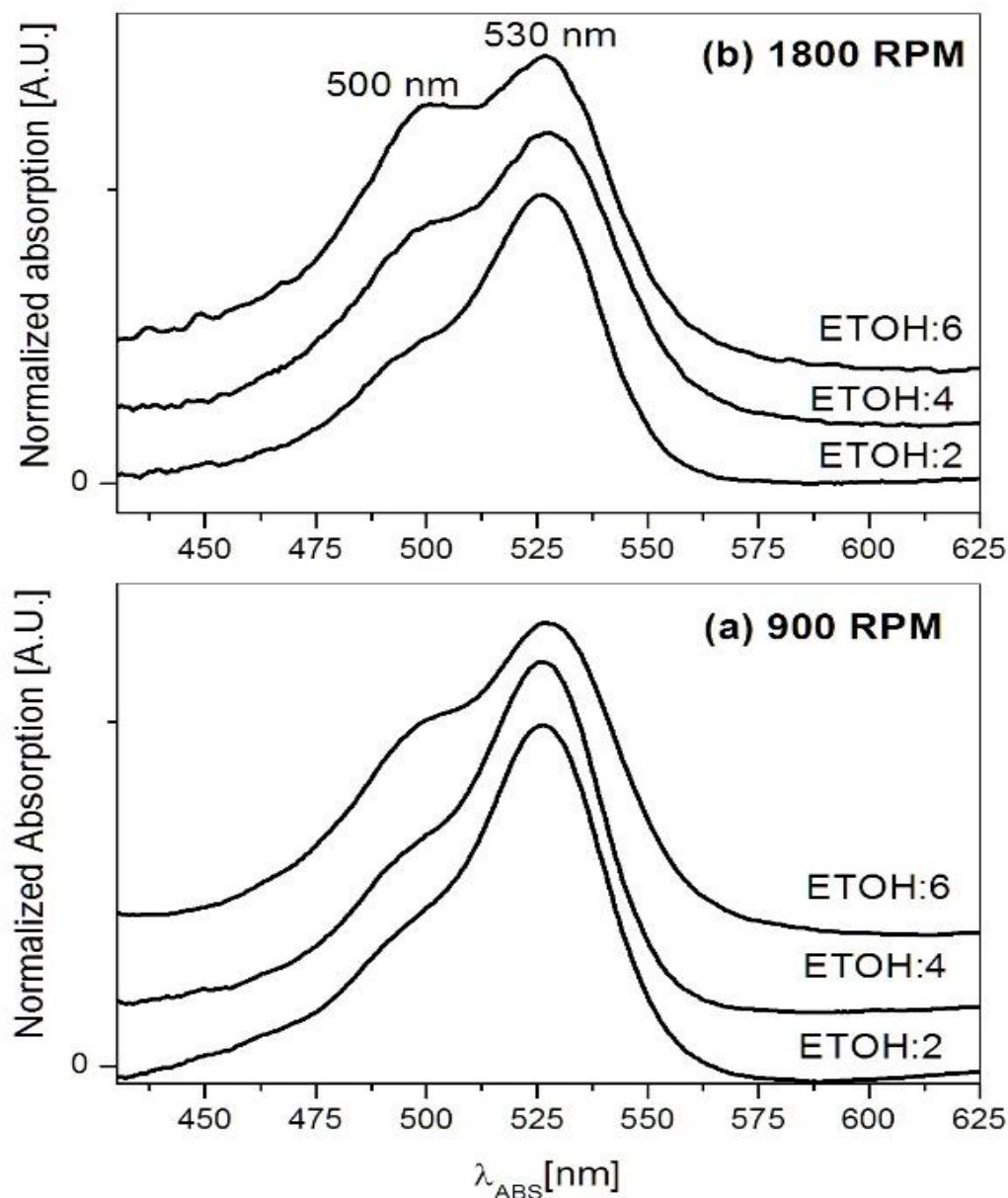


Figure 9. Absorption spectra of silica sol-gel thin films embedding Rh6G at different ethanol content. The films were synthesized by spin coating at (a) 900 rpm, and (b) 1800 rpm.

4. Conclusions

Macroporous sol-gel silica films embedding Rh6G were synthesized by spin-coating. The presence of the pores on the film surface was attributed to the aggregation of Rh6G in the film composition. The evaporation rate during spin coating is a factor that determined the pore size distribution. This was accomplished by varying the rotation speed and the solvent content. For the former, higher rpm lead to smaller size pores. On the other hand, at higher ETOH content. the subsequent reduction of the viscosity allowed larger pore diameters. The monomeric form of the Rh6G was the main aggregate in the films. However, H-type dimers also appeared for higher solvent content, which is also related to the formation of wider macro pores in our films at certain extent.

References

- Ashrafi-Shahri, S. M., Ravari, F., & Seifzadeh, D. (2019). Smart organic/inorganic sol-gel nanocomposite containing functionalized mesoporous silica for corrosion protection. *Progress in Organic Coatings*, 133, 44-54. <https://doi.org/10.1016/j.porgcoat.2019.04.038>
- Bao Y., Wang T., Kang Q. Shi C., & Ma J. (2017). Micelle-template synthesis of hollow silica spheres for improving water vapor permeability of waterborne polyurethane membrane. *Scientific Reports* 7(1), 46638. <https://doi.org/10.1038/srep46638>
- Bhar R, Kanwar R., & Mehta S.K. (2020), Surface engineering of nanoparticles anchored meso-macroporous silica heterostructure: An efficient adsorbent for DNA. *Materials Chemistry and Physics* 255. 123541 <https://doi.org/10.1016/j.matchemphys.2020.123541>
- Corma A. (1997). From Microporous to Mesoporous Molecular Sieve Materials and Their Use in Catalysis. *Chemical Reviews*. 97(6), 2373-2420. <https://doi.org/10.1021/cr960406n>
- Gaspera E. D., & Martucci A. (2015). Sol-Gel Thin Films for Plasmonic Gas Sensors. *Sensors* 15(7), 16910-16928. <https://doi.org/10.3390/s150716910>
- Gibaud A., Grosso D., Smarsly B., Baptiste A., Bardeau J. F., Babonneau F., Doshi D. A., Chen Z., Brinker C. J., & Sanchez C. (2003). Evaporation-Controlled Self-Assembly of Silica Surfactant Mesophases. *Journal of Physics Chemistry. B.* 107 (25), 6114-6118. <https://doi.org/10.1021/jp027612l>
- Hanczyc P., Sznitko L., Zhong C., & Heeger A. J. (2015). Stimulated Emission from Rhodamine 6G Aggregates Self-Assembled on Amyloid Protein Fibrils. *ACS Photonics*, 2(12), 1755-1762. <https://doi.org/10.1021/acsphotonics.5b00458>
- Herzog N., Hübner H., Rüttiger C., Gallei M., & Brunsen A. (2020). Functional Metalloblock Copolymers for the Preparation and In Situ Functionalization of Porous Silica Films. *Langmuir* 36(15), 4015-4024. <https://doi.org/10.1021/acs.langmuir.0c00245>
- Leonenko E., Telbiz G., Bogoslovskaya A. & Manoryk P.A. (2015). Effect of Aggregation of Rhodamine 6G on the Spectral and Luminescence Characteristics of Hybrid Mesostructured Silica Films. *Theoretical and Experimental Chemistry* 50, 358-363 <https://doi.org/10.1007/s11237-015-9388-8>
- Li C., Li Q., Kaneti Y. V., Hou D., Yamauchi Y., & Mai Y. (2020). Self-assembly of block copolymers towards mesoporous materials for energy storage and conversion systems. *Chemical Society Reviews*. 49, 4681-4763. <https://doi.org/10.1039/D0CS00021C>
- Malfatti L., Kidchob T., Aiello D., Aiello R., Testa F., & Innocenzi P. (2008). Aggregation States of Rhodamine 6G in Mesostructured Silica Films. *The Journal of Physical Chemistry C*, 112(42) 16225-16230. <https://doi.org/10.1021/jp801392f>
- Mubarekyan E., & Santore M. (1998). Characterization of Polystyrene Latex Surfaces by the Adsorption of Rhodamine 6G. *Langmuir*, 14(7), 1597-1603. <https://doi.org/10.1021/la970855y>
- Narang, U., Wang, R., Prasad, P. N., & Bright, F. V. (1994). Effects of aging on the dynamics of rhodamine 6G in tetramethyl orthosilicate-derived sol-gels. *The Journal of Physical Chemistry*, 98(1), 17-22. <https://doi.org/10.1021/j100052a005>

- Nasr, C., Liu, D., Hotchandani, S., & Kamat, P. V. (1996). Dye-capped semiconductor nanoclusters. Excited state and photosensitization aspects of rhodamine 6G H-aggregates bound to SiO₂ and SnO₂ colloids. *The Journal of Physical Chemistry*, 100(26), 11054-11061.
<https://doi.org/10.1021/jp9537724>
- Phan, T. T. N., Nikoloski, A. N., Bahri, P. A., & Li, D. (2019). Facile fabrication of perovskite-incorporated hierarchically mesoporous/macroporous silica for efficient photoassisted-Fenton degradation of dye. *Applied Surface Science*, 491(15), 488-496.
<https://doi.org/10.1016/j.apsusc.2019.06.133>
- Nishikiori H., & Fujii T. (1997). Molecular Forms of Rhodamine B in Dip-Coated Thin Films. *Journal of Physical Chemistry B*, 101(19). 3680-3687.
<https://doi.org/10.1021/jp962734x>
- Pan J. H., & Lee W.I. (2005). Selective control of cubic and hexagonal mesophases for titania and silica thin films with spin-coating. *New Journal of Chemistry*. 29(6), 841-846.
<https://doi.org/10.1039/B417310D>
- Roushani M., & Ghanbari K. (2019). An electrochemical aptasensor for streptomycin based on covalent attachment of the aptamer onto a mesoporous silica thin film-coated gold electrode. *Microchimica Acta* 186 (115).
<https://doi.org/10.1007/s00604-018-3191-x>
- Wu P. H., Mäkie P., Odén M., & Björk E. M. (2019) Growth and Functionalization of Particle-Based Mesoporous Silica Films and Their Usage in Catalysis. *Nanomaterials: Functional Nanoporous Materials*, 9(4), 562-574
<https://doi.org/10.3390/nano9040562>
- Yamashita H., Mori K., Kuwahara Y., Kamegawa T., Wen M., Verma P., & Che M. (2018). Single-site and nano-confined photocatalysts designed in porous materials for environmental uses and solar fuels. *Chemical Society Reviews* 47, 8072.-8096
<https://doi.org/10.1039/C8CS00341F>
- Yang J., Lin G., Mou C. Y., & Tung K. L. (2019), Diatom-Mimicking Ultrahigh-Flux Mesoporous Silica Thin Membrane with Straight-Through Channels for Selective Protein and Nanoparticle Separations. *Chemistry of Materials*. 31(5), 1745-1751.
<https://doi.org/10.1021/acs.chemmater.8b05295>
- Zhang J., Meng Z., Liu J., Schlaich C., Yu Z., & Deng X..(2017). Breath figure lithography for the construction of a hierarchical structure in sponges and their applications to oil/water separation. *Journal of Materials Chemistry A*, 5(31), 16369-16375.
<https://doi.org/10.1039/C7TA02751F>